Near-field relaxation subsequent to the onset of oblique detonations with a two-step kinetic model

Honghui Teng (滕宏辉) [1], Hoi Dick Ng [2], Pengfei Yang (杨鹏飞) [3,4,*] and Kuanliang Wang (王宽亮) [1]

[1] School of Aerospace Engineering, Beijing Institute of Technology, Beijing 100081, China

[2] Department of Mechanical, Industrial and Aerospace Engineering, Concordia University, Montreal, QC, H3G 1M8, Canada

[3] State Key Laboratory of High Temperature Gas Dynamics, Institute of Mechanics, Chinese Academy of Sciences, Beijing 100190, China

[4] School of Engineering Sciences, University of Chinese Academy of Sciences, Beijing 100049, China

Abstract: Initiation of oblique detonation wave (ODW) results in a near-field region of curved detonation wave surface, which cannot be predicted by the detonation polar theory and lacks of in-depth work on its features. In this study, Euler equations coupled with a two-step kinetic model are used to simulate ODW dynamics, and then the flow structures are analyzed by examining the asymptotic decay of local surface angle (LSA) and the flow/reaction coupling along streamlines quantified by a non-dimensional Damköhler number Da_s. The results demonstrate a spectrum of local strong solutions forms, which always happens when the ODW transition pattern is abrupt, but the strong solutions deviate from the isolated strong solution predicted by the polar theory. Furthermore, the abrupt transition leads to a strong peak of Da_s, defined by the ratio of the characteristic flow and chemical reaction length, while the smooth one leads to a bump. Various simulated cases indicate that the transition pattern becomes abrupt and the local strong solution arises when the maximum Da_s reaches a critical range.

Key words: Oblique detonation, solution multiplicity, strong solution, subsonic region

* Author to whom correspondence should be addressed: young1505@foxmail.com

Ⅰ. INTRODUCTION

For aerospace propulsion systems, detonation as a form of pressure-gain combustion has the potential to deliver high thermodynamic efficiency and low mechanical complexity. Among different gaseous detonation configurations, oblique detonation waves (ODWs) whose front is not perpendicular to the incoming flow similar to oblique shock waves (OSWs), can be stabilized by wedges or blunt bodies. The idea of harnessing a standing ODW has long been proposed[1,2] and has been the topic of extensive investigations, focusing primarily on the wave structure[3–6] and surface instability[7–9]. Furthermore, ODWs influenced by various realistic flow scenarios have been studied relating to practical applications, such as effects of the finite-length wedge[10–13], nonuniform mixtures[14] and unsteady inflows[15].

The ODW initiation occurs in a distinct region persisting in the combustor chamber, differed from pulse or rotating detonation engines[16–20]. Thus, research on the ODW initiation is crucial to achieving stable and efficient combustion. The ODW initiation is characterized by a transition from oblique shock to detonation on the surface, either smoothly or abruptly, and leads to complicated wave configurations beneath the surface transition region[5,21]. The combustion in supersonic flow may involve the interaction of compression waves, contact surface and reactive front[22–25]. In early works, the wave configuration was usually described by a steady multi-wave structure issued from a triple initiation point[3, 26]. Meanwhile, the difference between smooth and abrupt transition has been investigated, and some models on the transition type have been proposed based on the flow field analysis[5,6]. However, these models are usually limited in a parametric range, because they are semi-empirical without substantial research on the wave configuration. Recently, some new wave configurations were observed benefiting from high-resolution numerical simulations. For instance, the combination of compression waves, oblique shock and normal shock has been observed as the wave system of ODW in argon diluted acetylene-oxygen mixtures[27]. A semi-theoretical approach to shed light on the wave systems of ODWs at the initiation region and four types of wave systems are analyzed from the viewpoint of compression wave

convergence[28]. These new findings demonstrate that more detailed studies on the initiation region are necessary in order to get a full understanding of the wave configuration and stability.

The aforementioned studies concern primarily the wave configuration beneath the shock front transition region, but there is less attention to the transient, near-field ODW development. The initiation structure usually includes several waves, while the near-field ODW formed just downstream interacts closely with the wave configuration. Indeed, the complete ODW initiation is determined collectively by the type of wave configuration and subsequently the near-field ODW, yet only the former has been studied widely before. Previous theoretical works investigate the ODW surface by detonation polar analysis[29–31], but the near-field ODW is not applicable because the theoretical analysis assumes a straight detonation surface (or a fixed oblique angle) across which the flow is uniform. A straight surface is only applicable for the far-field ODW, while for the near-field ODW, a curved surface arises whose shock angle evolves and decreases gradually[32]. The decaying wave angle suggests that the near-field ODW is non-equilibrium and relaxing downstream. There is still a lack of quantitative variation rules of near-field ODWs so far, so the criteria on the transition features remain semi-empirical.

This study presents the simulated ODWs focusing on the near-field oblique detonation and its relaxation. The parameters adjusted include the Mach number, wedge angle and chemical reaction coefficient. By introducing the local surface angle (LSA), the decaying behavior of the near-field ODW surface has been analyzed. A spectrum of local strong solutions, which deviates from the isolated strong solution predicted by the polar theory, has been pointed out and its formation with the abrupt transition has been confirmed for the first time. On the other side, a non-dimensional Damköhler number Da_s has been defined as the ratio to quantify the flow/reaction coupling, whose variations provide a new viewpoint in the ODW research.

Ⅱ. PHYSICAL AND MATHEMATICAL MODELS

Following the canonical ODW simulation setting, the reactive Euler equations are used, coupled with a two-step ideal chemistry model simulating chain-branching kinetics[33]:

$$\dot{\omega}_1 = H(1-\xi)\rho k_I \exp\left[E_I\left(\frac{1}{T_S}-\frac{1}{T}\right)\right] \tag{1}$$

$$\dot{\omega}_2 = [1-H(1-\xi)]\rho(1-\eta)k_R \exp\left[-\frac{E_R}{T}\right] \tag{2}$$

where $\dot{\omega}_1$ and $\dot{\omega}_2$ represent the reaction rate of the induction zone and heat release zone, respectively; ξ and η represent respectively the progress variables for the induction and reaction step. The variable ξ changes from one to zero, and η has a value from zero to one. $H(1-\xi)$ is a Heaviside step function (1 when $\xi \le 1$ or 0 if $\xi > 1$) and the specific total energy e is given by $p/\rho(\gamma-1) + (u^2+v^2)/2 - \eta \cdot Q$. The symbols ρ, u, v, p and Q are the density, velocities in x- and y- direction, pressure, and heat release amount, respectively. The kinetic parameter of induction step k_I is chosen such that the one-dimensional Zeldovich–von Neumann–Döring (ZND) induction length is unity. The pre-exponential factor k_R, whose default value is 1.0, is employed here to vary the rate of heat release. All the flow variables have been made dimensionless by reference to the upstream flow state as follows (the superscript symbol (~) denotes original dimensional quantities and subscript symbol (0) indicates reference quantities ahead of the detonation/shock front):

$$p = \frac{\tilde{p}}{p_0},\quad \rho = \frac{\tilde{\rho}}{\rho_0},\quad T = \frac{\tilde{T}}{T_0},\quad u = \frac{\tilde{u}}{\sqrt{RT_0}},\quad v = \frac{\tilde{v}}{\sqrt{RT_0}},\quad Q = \frac{\tilde{Q}}{RT_0} \tag{3}$$

The heat release amount Q and specific heat ratio γ are taken as 25 and 1.2, respectively. The corresponding propagation Mach number of one-dimensional Chapman–Jouguet (CJ) detonation is 4.5. Dimensionless activation energies used in this study are E_I = 4.0 T_S, E_R = 1.0 T_S, where T_S is the temperature jump across the leading shock of one-dimensional CJ detonation. The activation energies E_I and E_R have been scaled with RT_0. The symbol R is gas constant, and T_0 is the temperature of free inflow. The typical value of the induction activation energy usually ranges from 4 Ts to

12 *T*s for hydrogen/hydrocarbon mixtures[33]. The dimensionless heat release Q is related to the free inflow state and generally ranges from 10 to 50. Even though the chosen chemical parameters in this study do not correspond to any specific fuel, these model parameters can reproduce generic detonation combustion characteristics and have been examined by many previous studies[1,6,7,30,33].

The governing equations are discretized on Cartesian uniform grids and solved with the dispersion-controlled dissipation (DCD) scheme[34] together with a third-order Runge-Kutta algorithm. The DCD scheme is designed to adjust the dispersion around the strong discontinuity and thus, non-physical oscillations near the shock wave are suppressed. Generally, it is one kind of total variation diminishing (TVD) schemes, which can achieve second-order accuracy in the smooth flow field. A rectangular cartesian grid in the computational domain is aligned with the wedge surface (see Fig. 1). The coordinate frame is rotated to the direction along the wedge surface, which could avoid the potential staircasing issues.

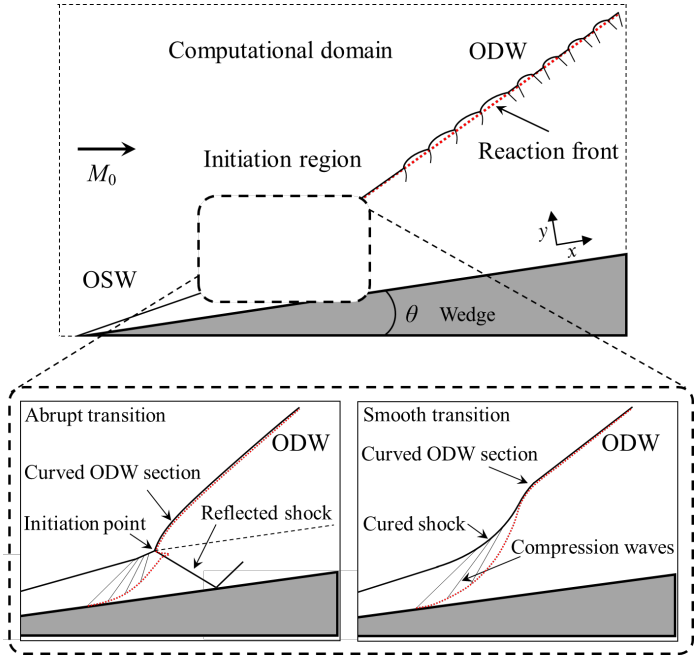

FIG. 1. The schematic of ODW induced by a wedge.

The initial parameters of the computational domain are set to be the free inflow. The left and upper boundaries are modelled as inflow boundary conditions, where the parameters are fixed to be constant due to the supersonic flow. Outflow conditions extrapolated from the interior are implemented on the right boundary and lower

boundaries before the wedge. The slip boundary condition is used on the wedge surface, which starts from $x = 4.0$ on the lower boundary.

For the presence of the wedge in a supersonic inflow, an attached planar OSW is formed and subsequently evolves to an oblique detonation due to the high temperature behind the OSW triggering an exothermic chemical reaction. The OSW–ODW transition shown in Fig. 1 involves two types of wave structures dependent on inflow Mach number M_0 and wedge angle θ. The low M_0 and θ will lead to an abrupt OSW–ODW transition with a multi-wave point. It is also observed that the initiation structure depends on the M_0 and θ, identical to the previous studies[3,6].

To extract the flow features of near-field ODWs, the LSA and Da_s have been proposed in this study. The method of determining the LSA and the definition of the non-dimensional number Da_s are given in Appendix A. The former gets the variation rule of oblique surfaces, illustrating the decaying process of the detonation front. The latter calculates the flow and reaction characteristic lengths, quantifying the flow/reaction coupling relation.

Ⅲ. RESULTS AND DISCUSSION

A. Structure variation with respect to M_0 and θ

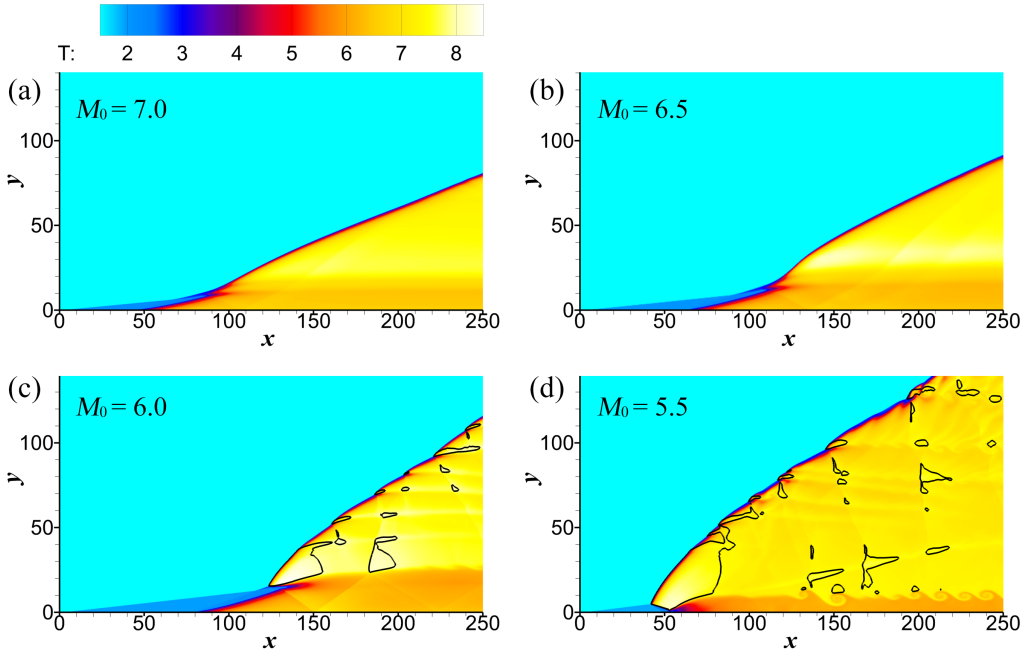

FIG. 2. Temperature fields and sonic curves (black contours) of ODW with $\theta = 25°$, $k_R = 1.0$ and M_0 = (a) 7.0, (b) 6.5, (c) 6.0, (d) 5.5.

To start with, a group of ODWs has been simulated by changing M_0, whose temperature fields are displayed in Fig. 2. As M_0 decreases, the smooth transition changes to an abrupt type, and simultaneously the detonation wave front becomes wrinkled with triple points forming on the surface. One can see that from Figs. 2(a)–(c), the ODW initiation location moves downstream. This is because the lower post-OSW temperature reduces the reaction rate, and the mixture needs more time to release chemical energy. Besides, the velocity behind the OSW has a slight decrease, due to the decreasing M_0 of the inflow. These two factors cause the increase in the initiation length. When the M_0 decreases to 5.5, as shown in Fig. 2(d), the detonation front angle increases further and the initiation location moves upstream unexpectedly. A similar phenomenon has been observed in a previous study[21] in which the structural shift of ODW is vaguely attributed to the combination of detonation instability and reaction rate. The intrinsic mechanism dominating the OSW–ODW transition structures remains

to be elucidated and will be discussed later.

Furthermore, the sonic curves are also plotted in Fig. 2 to pinpoint other salient features of ODWs. For the case with higher M_0, there are no subsonic zones, as shown in Figs. 2(a) and (b). However, there are several subsonic zones in Figs. 2(c) and (d), and the largest subsonic zone appear behind the initiation point in both cases. It is noted that the subsonic zone appears when the transition becomes abrupt, but whether this is a universal rule will be examined in the later part of this paper.

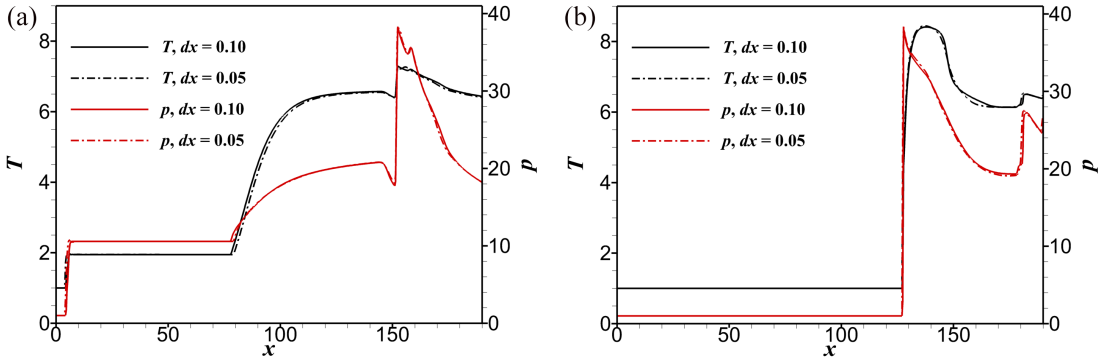

FIG. 3. Results of the resolution study along the line y = (a) 0 and (b) 20.

A grid-independence study is conducted to verify the "convergence" of the numerical results produced by the different square grid length scales, namely, 0.1 and 0.05. As mentioned above, the induction length of one-dimensional ZND detonation is unity. The grid scale dx = 0.1 or 0.05 means that there are 10 or 20 points in the ZND induction length. Since the ODW front is not perpendicular to the incoming flow, the flow patch distance is greater than the ideal induction length. In this sense, the number of mesh points per induction length in ODW flow fields is greater than the one-dimensional detonation wave. The general ODW structures with different grids are essentially the same except for a slight difference in the pressure contours in the combustion products. Hence, the finer flow fields are not shown here. To provide a further quantitative comparison, the temperature and pressure profiles along with the wedge-parallel lines y = 0 and 20 are also shown in Fig. 3, which corresponds to the inflow conditions of Fig. 2(c). The curves overlap each other and the differences are hardly distinguishable. Furthermore, we calculated the temperature/pressure deviations

of different grid scales according to the results of Fig. 3. The maximum deviation is about 3.0% and mainly occurs near the detonation front. The deviation of the post-shock flow state is generally less than 1.0%. In Fig 3(a), the low temperature behind the oblique shock results in a long induction length, followed by the modest pressure and temperature increases downstream. A temperature/pressure peak is also observed, induced by the reflection of the oblique shock produced from the multi-wave point. Along the line y = 20, the post-shock temperature is high and in turn sufficient to establish an overdriven detonation. The temperature and pressure rise steeply at the same time, indicating a strong coupling between the shock and heat release. Here, the default grid-scale, i.e., dx = 0.1, is proven to provide good converged initiation structures, sufficient to guarantee the reliability of the conclusions, and is thus used subsequently in the present work.

Three angles (β_S, β_D, and β_W) predicted by the detonation/shock polar theory have been plotted, whose calculation method and detailed values are listed in Appendix B. Notably, the detonation surface angles based on the polar theory are not directly applicable in the prediction of local ODW surface angle. This is because that the flow of the initiation zone is in a nonuniform and non-equilibrium state. Hence, the predicted angles are only provided as a guide for the simulated results. By contrast, the differences between the numerical approach and theoretical method can be described quantitatively. More importantly, the decaying process of after-initiation for the ODW can be shown by the LSA variations. Many of the key dynamic parameters, e.g., decaying length and overdriven degree, are easily obtained by the LSA features[32]. Given M_0 and θ, the wave angles β_S and β_W denote the strong and the weak solution, respectively. The angle β_D corresponds to the detached angle of the wedge-induced ODW, beyond which the detonation will detach from the wedge surface.

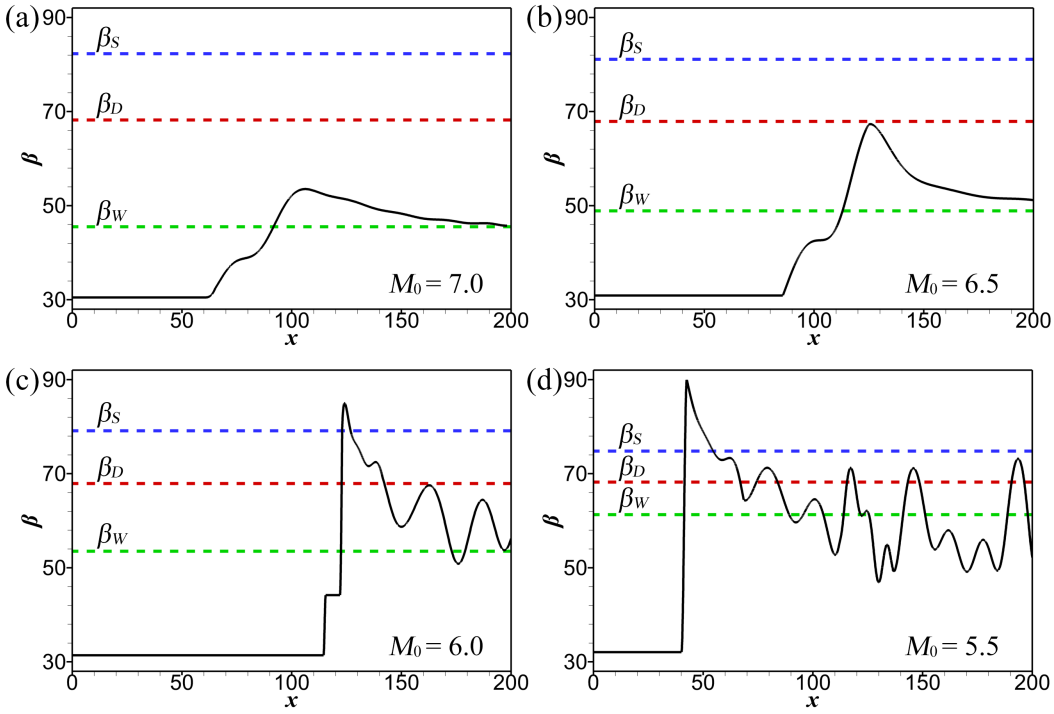

FIG. 4. Comparison of the numerical LSA with the theoretical angles from the detonation polar with $\theta = 25°$, $k_R = 1.0$ and M_0 = (a) 7.0, (b) 6.5, (c) 6.0, (d) 5.5.

As shown in Fig. 4(a), a continuous rising of the LSA is observed, whose maximum value is noticeably higher than β_W. More specifically, the LSA shows a constant angle before x = 60 which corresponds to the OSW angle, followed by a smooth two-stage similar increase due to the heat release from the ODW initiation process. In theory, the heat release under a supersonic flow could trigger a series of compression waves. These pressure waves interact with the leading OSW and lead to a first-step continuous increase. The second stage corresponds to the detonation initiation process, in which the reaction front is getting close to the curved shock wave and the LSA presents an increase again. After reaching the maximum value, the LSA then decays gradually to β_W. A relaxation process towards the equilibrium angle is clearly seen, demonstrating that the flow near the initiation region is nonuniform and cannot be predicted by the detonation polar theory. In the case of M_0 = 6.5, a similar curve of LSA variation is observed, but the maximum angle becomes higher, close to the detached angle β_D. Decreasing M_0 to 6.0, the LSA change at the initiation region becomes a clear two-step discontinuity. This abrupt two-step LSA increase is evolved from the previous LSA

curves with the two-stage modest rising seen in Figs. 4(a) and (b). More importantly, the peak of this LSA curve in Fig. 4(c) not only overwhelms β_D but also β_S. In Fig. 4(d) with $M_0 = 5.5$, the LSA peak is close to 90°, leading to almost a normal detonation there. Recalling that the subsonic zone appears in these two cases [see Figs. 2(c) and (d)], it could be concluded that the strong solution branch is first achieved locally. After the strong solutions in both cases, the LSA decays to and oscillates roughly around β_W, as shown in Figs. 4(c) and (d). It should be repeated that the far-field cellular surface leads to a challenge to get the front angle of ODW from the discrete data points. Besides, the oscillation features of far-field detonation surfaces have been reported in previous studies[32] by analyzing the pressure evolutions. This study focuses on the near-field initiation structures and the formation of local strong solutions as a precursor to the onset of the abrupt transition. Hence, the LSA variations of the downstream flow field exhibiting irregular structures are not discussed here.

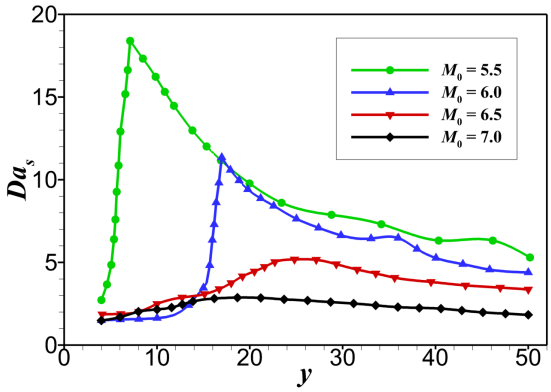

FIG. 5. Da_s of ODW with $\theta = 25°$, $k_R = 1.0$ and various M_0 values.

The decaying of LSA displays a relaxing process of the local strong over-driven detonation, in which the overdrive degree decreases, coupled with the onset of instability and successively the formation of cellular structures. From another viewpoint, the coupling of flow and reaction also changes, whose variation could be analyzed in Fig. 5 through Da_s of ODW fronts. As mentioned earlier, Da_s is used in this work to describe the flow/reaction coupling along the streamline. Theoretically, Da_s equals 1.0 for the far-fields of ODW, which has been proven using the case of $M_0 = 7.0$ and $\theta = 30°$ (see Appendix A).

Overall, Da_s rapidly reaches its maximum value after initiation and then drops slowly, as shown in Fig. 5. More importantly, there is a significant difference between the smooth transition ODW (M_0 = 7.0 and 6.5) and the abrupt one (M_0 = 6.0 and 5.5). The smooth ODWs result in a continuous change in Da_s, while the abrupt ones lead to the apparent formation of the peak. Besides, the maximum Da_s value increases sharply as M_0 decreases. Associated with the peak formation, a large subsonic zone forms behind the initiation point. A low M_0 corresponds to a higher peak of Da_s, and the downstream detonation front needs more time-space to relax to a final equilibrium state. The analysis of Da_s provides a new viewpoint on the formation of local strong solutions in ODWs which has not been introduced before. Besides, the multi-wave structures on the surface are changing continually and it is very difficult to define the flow length L_f of the unstable detonation front precisely. Hence, the Da_s variations of the downstream irregular structures are not discussed here.

B. Discussion on critical structures

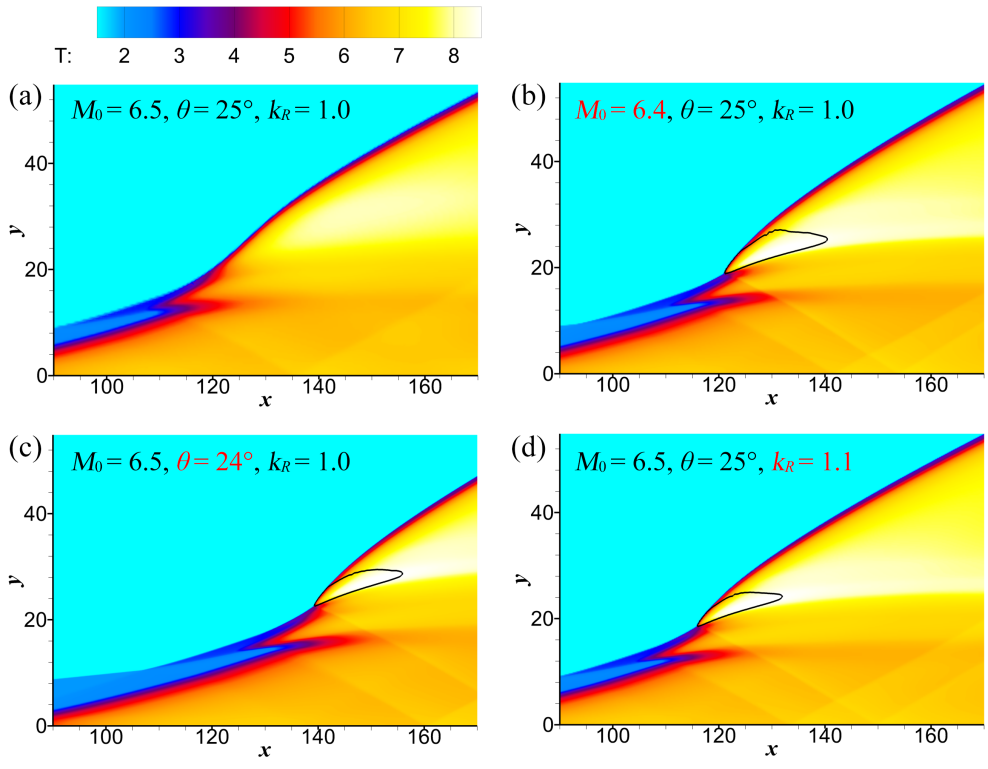

FIG. 6. Temperature fields and sonic curves (black contours) of the ODWs. The

basic case is (a) $M_0 = 6.5$, $\theta = 25°$, $k_R = 1.0$. The critical cases are obtained by varying (b) $M_0 = 6.4$; (c) $\theta = 24°$; (d) $k_R = 1.1$.

The above results demonstrate that the occurrence of local subsonic zones in the ODW influences the LSA and Da_s substantially, but it is still unclear whether these phenomena are universal or just happen by chance. Therefore, we have explored some cases by varying the controlling parameters systematically, leading to the critical structures in which the subsonic zone just appears. Common features of these critical structures would be vital to deepen our understanding of the ODW morphology. The first case group is based on the conditions of $M_0 = 6.5$, $\theta = 25°$ and $k_R = 1.0$, whose flow field has been displayed in Fig. 2(b). Three critical structures by varying M_0, θ or k_R are simulated and shown in Fig. 6. We find that the case of $M_0 = 6.5$, $\theta = 25°$ and $k_R = 1.0$ is close to the critical structures, so a slight decrease in certain parameters (M_0, θ and k_R) can result in a critical structure. As shown in Figs. 6(b)–(d), the common feature is that there a subsonic zone near the initiation region. Compared to the result of Fig. 6(a), the OSW–ODW transition of the critical structure is achieved via a multi-wave initiation point.

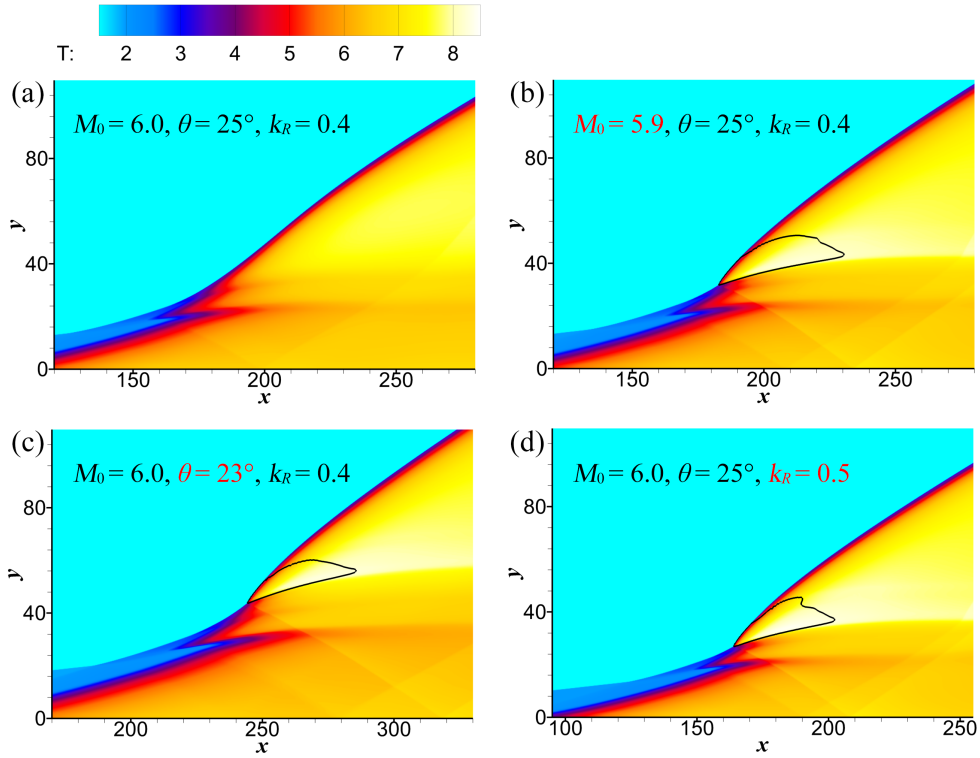

FIG. 7. Temperature fields and sonic curves (black contours) of the ODWs. The basic case is (a) $M_0 = 6.0$, $\theta = 25°$, $k_R = 0.4$. The critical cases are obtained by varying (b) $M_0 = 5.9$; (c) $\theta = 23°$; (d) $k_R = 0.5$.

The second group of cases is based on $M_0 = 6.0$, but it is difficult to get the critical structure by varying the parameters of the case shown in Fig. 2(c). This is because the present structure of Fig. 2(c) is far away from the critical structure. By fixing the same M_0 and θ, we decrease k_R to be 0.4 and then a basic structure arises, as shown in Fig. 7(a). Thereafter, three other critical structures are obtained by varying M_0, θ and k_R. When M_0 decreases to be 5.9, a subsonic zone occurs behind the initiation point, which results in a critical structure. While the flow structures are relatively insensitive to the wedge angle θ, there are still no subsonic zones in the case of $\theta = 24°$. The critical structure appears only when θ decreases to be 23°. Increasing k_R slightly to 0.5 leads to a critical structure. To compare the features among them, these results are displayed in Fig. 7. Three types of parameters, involving the gas-dynamics, geometry and chemistry, dominate the appearance of the subsonic zone in the detonation product. As mentioned above, the occurrence subsonic zone is usually associated with a sudden shift in LSA and Da_s of wave front near the initiation region. Thus, we will analyze the relationship of the LSA, Da_s and the subsonic zone in the following part.

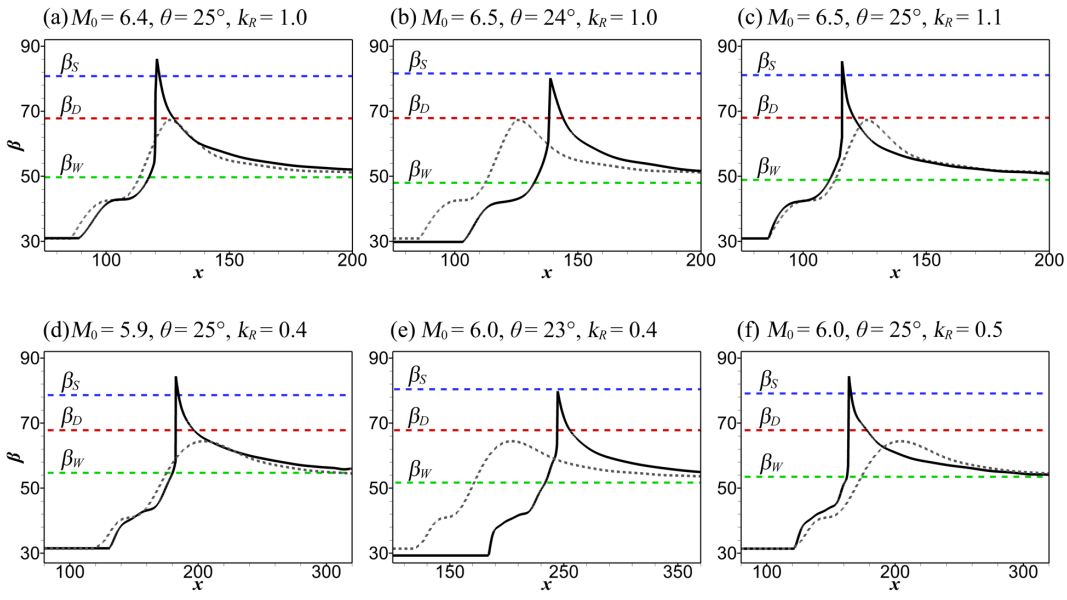

FIG. 8. LSA curves of critical ODWs. In the first row, the grey dashed lines denote

the case of $M_0 = 6.5$, $\theta = 25°$, $k_R = 1.0$; the black solid lines denote the cases obtained by varying (a) $M_0 = 6.4$; (b) $\theta = 24°$; (c) $k_R = 1.1$. In the second row, the grey dashed lines denote the case of $M_0 = 6.0$, $\theta = 25°$, $k_R = 0.4$; the black solid lines denote the cases obtained by varying (a) $M_0 = 5.9$; (b) $\theta = 23°$; (c) $k_R = 0.5$.

Based on the two groups of cases, corresponding to the results of Figs. 6 and 7, the LSA variations are calculated and displayed in Fig. 8. For comparison, the LSA of the reference case is also plotted by a grey dashed line in each frame. Three wave angles of β_S, β_D and β_W in each frame are calculated respectively using their own M_0 and θ. As demonstrated in Fig. 8, almost all the LSA curves undergo a two-stage increase in the initiation process. After the maximum value induced by initiation, the LSA decreases slowly and finally tends to the constant β_W (the weak solution). Since the detonation front near the initiation region is curved, the flow is nonuniform and involves the interactions of different waves and heat release. Benefiting from the LSA curves, we can see that the critical structure of ODW leads to a peak of LSA value (the black solid lines in Fig. 8) and the corresponding maximum value is greater than the detached angle β_D.

Recalling the resulting ODWs fields shown in Figs. 6 and 7, the subsonic zone occurs in all critical cases, in which the OSW–ODW transition type is known as the abrupt one. When the detonation front angle is greater than β_D, a subsonic zone forms near the initiation point. In other words, the theoretical detached wave angle β_D could be used as a quantitative criterion of smooth and abrupt transition patterns. These findings may indicate that the abrupt transition pattern equals the presence of the subsonic zone physically. Note that the strong solution is not equivalent to the formation of a subsonic zone. The criterion of the strong solution is the detached wave angle β_D. However, the detached wave angle β_D cannot be used to distinguish the presence of the subsonic zone. This is because that when the wave angle is very close to the angle β_D, it is theoretically possible that the post-shock flow is still subsonic regardless of strong and weak solutions [30].

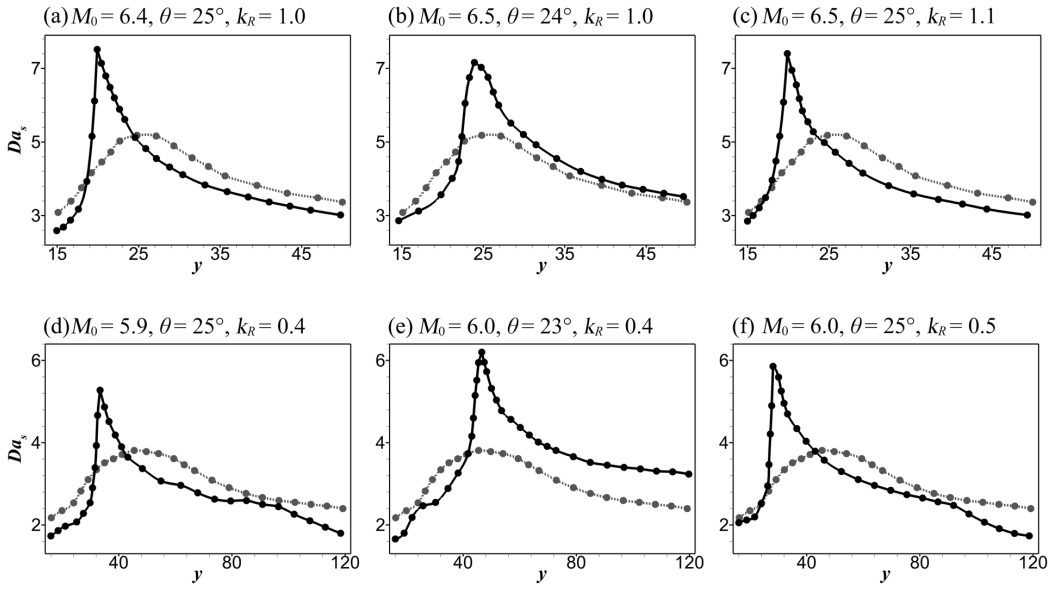

FIG. 9. Da_s curves of critical ODWs. In the first row, the grey dashed lines denote the case of M_0 = 6.5, θ = 25°, k_R = 1.0; the black solid lines denote the cases obtained by varying (a) M_0 = 6.4; (b) θ = 24°; (c) k_R = 1.1. In the second row, the grey dashed lines denote the case of M_0 = 6.0, θ = 25°, k_R = 0.4; the black solid lines denote the cases obtained by varying (a) M_0 = 5.9; (b) θ = 23°; (c) k_R = 0.5.

The present analysis pays further attention to Da_s curves of critical ODWs, as shown in Fig. 9. The grey dashed lines denote the Da_s variation of the reference cases, in which the OSW–ODW transition type is smooth. It is observed that Da_s always reaches its maximum value shortly after initiation, and the abrupt transition leads to a strong peak while the smooth one leads to a bump. The initial increase in Da_s corresponds to the detonation initiation process and the decaying part corresponds to the relaxation of overdriven ODWs. It is noted that when the maximum Da_s reaches about 5~7, the transition becomes abrupt and the local strong solution arises. As mentioned above, the sudden shift in the value of Da_s means a significant change in flow nature, i.e., the flow behind the shock becomes subsonic. By introducing the Da_s of the ODW, the common flow features of the initiation region by different parameters (M_0, θ, and k_R) are confirmed once more.

Although all three parameters can lead to a similar subsonic zone in the detonation product, their effect on the downstream detonation wave is a little bit different. In Figs.

9 (a) and (d), the decreasing M_0 brings about a peak value of Da_s, which becomes lower downstream compared to the grey line. A similar phenomenon can be observed in Figs. 9 (c) and (f). However, the abrupt transition obtained by decreasing θ not only leads to a peak near the initiation region but also a higher Da_s of the downstream ODW, as shown in Figs. 9 (b) and (e). These differences may be attributable to a change in the initiation point. The decreasing M_0 or increasing k_R results in the fact that the initiation point of the abrupt ODW is located at the left side compared to the smooth transition case, while the initiation point remains basically unchanged for the varying θ. Besides, the Da_s for all cases asymptote to 1.0 in theory. However, the overdrive degree of detonation front decreases along with the relaxation process. The onset of surface instability and cellular structures leads to the fluctuation of Da_s for the downstream detonation wave.

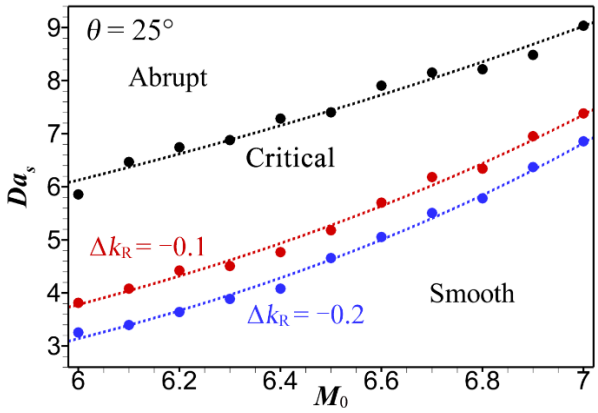

FIG. 10. The maximum Da_s value of critical ODWs with different M_0.

Notably, although the simulated results are based on a two-step induction–reaction model, the smooth and abrupt transitions have been observed with many chemical kinetic models[5,6,10,21], e.g., one-step model, two-step model, three-step model and detailed reaction model. The quantitative results may be affected by the chemical model[35], but the main findings and analysis methods proposed in this study can provide positive, worthwhile information for ODW research in the future. To further display the influence of chemical model parameters, the maximum Da_s value of critical ODWs with different M_0 is shown in Fig. 10 and the reference value of k_R is 1.0. The wedge angle is fixed to be 25°, and the critical cases are achieved by varying k_R with two

different increments Δk_R. Even though the heat release amount and reaction rate are partly linked, the rate k_R variability is in the range of 10% ~ 20% in Fig. 10. The slight variation in k_R has a limited effect on the heat release amount in a real reactive mixture. Hence, we keep the total heat release fixed and reduce the pre-exponential factor k_R. The main qualitative findings and analysis methods proposed in this study are still reliable. The situation that the reaction rate is reduced slightly and the heat release amount remains almost unchanged, could be realized by introducing a little bit of inert gas or catalyst.

The filled dots denote the data obtained from the resulting flow fields, and the dashed curves are fitted from the discrete data points based on the exponential function. It can be seen from the data in Fig. 10 that the maximum Da_s of the two transition types increases gradually as the M_0 increases. When the Da_s is below the red dashed line, a smooth OSW–ODW transition with a curved shock front is formed. Above the black dashed line, an abrupt transition occurs. Due to the difference between the smooth and abrupt structure, Da_s can change abruptly at the transition even a small increment Δk_R is used and hence, there is a region bounded by the two critical curves (i.e., red and black dashed lines) where no data value is found in all simulated cases. Furthermore, the heat release Q and activation energy E_R are also key model parameters. Similar to the factor k_R, the variation of activation energy E_R primarily affects the rate of heat release, as shown in Eq. (2). An increase in heat release Q is more beneficial to the presence of abrupt type[12]. If the value of Q or E_R is adjusted with different increments ΔQ or ΔE, a similar Da_s vs. M_0 map will be obtained. Compared to the situation with a variable k_R, a decrease in heat release Q or activation energy E_R leads to a decrease in the maximum Da_s near the initiation region, which means the drop of the boundary curves. While the trend of the boundary curves depends largely on M_0.

In most previous studies[3,5,6,10,29], the transition type is mainly distinguished by the presence of triple point near the initiation region and lacks of a quantitative criterion. In this study, the LSA and Da_s are introduced to analyze the decaying behavior of local surface angle and the flow/reaction coupling along streamlines and then used to find the physical relations between the abrupt transition ODW and the subsonic zone.

According to the present results, the OSW–ODW transition type can be defined by the presence of the subsonic zone. Meanwhile, the detonation surface is greater than the detached wave angle β_D. Moreover, the developed methods and the viewpoints of relaxation represented by LSA and Da_s would be helpful to advance the quantitative studies on the ODWs.

Ⅳ. CONCLUSIONS

In this study, Euler equations coupled with a two-step kinetic model are used to investigate the relaxation of near-field ODW. This ODW section cannot be predicted by the detonation polar theory, because the surface is curved and the post-surface flow is non-uniform. The simulated ODWs are analyzed from two aspects quantitatively: the decaying process of local surface angle (LSA) and the flow/reaction coupling along streamlines. Three parameters are adjusted to get different ODWs, including M_0, θ, and k_R representing the gas-dynamic, geometrical and chemical parameters, respectively. The parameters have been adjusted systematically to obtain the critical structures, from which the common key features of different ODWs could be distinguished. From the viewpoint of LSA decay, a spectrum of local strong solutions near the detonation initiation region has been observed and its existence with the abrupt transition has been confirmed for the first time. By defining a non-dimensional Damköhler number Da_s, it is observed that Da_s always reaches its maximum value shortly after initiation, and the abrupt transition leads to a strong peak while the smooth one leads to a bump. The critical structures indicate that when Da_s reaches a certain range, the transition becomes abrupt. Meanwhile, the maximum value of LSA exceeds the theoretical detached wave angle β_D and a local subsonic region occurs. Further parametric studies also show that the critical range will extend as the inflow Mach number increases.

ACKNOWLEDGEMENTS

This research was supported by the National Natural Science Foundation of China

(NSFC Nos. 12002041; 11822202), the Natural Sciences and Engineering Research Council of Canada (NSERC) and the 111 Project (No. B16003) of China.

APPENDIX A: ANALYSIS METHODS ALONG WAVE SURFACE AND STREAMLINE

To conduct the surface decay analysis, the LSA should be calculated first because the oblique detonation angle is not a constant but varies significantly along the wave surface. Determining the LSA from the simulated ODW flow fields presents a technical difficulty. Here, the simulation results are obtained numerically using a shock-capturing method, and the leading shock is unavoidably diffusive and not perpendicular to the mesh coordinates. An intuitive approach is to track the surface location along each y-axis parallel line, resulting in a list of shock heights as a function of the x-axis position. Nevertheless, such an approach often gives a step-like result as the shock height may not vary significantly in a certain range, even after the mending through interpolation inside the cell[8].

To analyze the LSA variation which is very sensitive to the smoothness of the function, a numerical method based on the polynomial curve fitting has been proposed and adopted in this study. The OSW/ODW fronts are obtained first along each y-axis parallel line, which can be implemented by monitoring the pressure/density increase. Since the shock front is a diffused interface in the numerical results, the locations of OSW/ODW fronts are defined as the points where the pressure increases to a value (reaches 110% of the inflow pressure) along lines parallel to the y-axis. Afterward, the collected discrete 2-D data points (x, y) are fitted using a high order polynomial (practically above 3rd-order) based on the generalized least squares (GLS)[36,37]. The fitting quality could be adjusted by choosing a proper degree of the polynomial. For the ODW flow field with complex structures, the discrete points are segmented into several groups according to the physical characteristics of the wave front, such as the oblique/curved shock, smooth surface and cellular surface. Each of these point groups has its own corresponding polynomial curve which is determined by the complex

processes of the wave structures. Using this numerical approach, we can obtain the slope/angle of the wave front by simply finding the derivative of the polynomial.

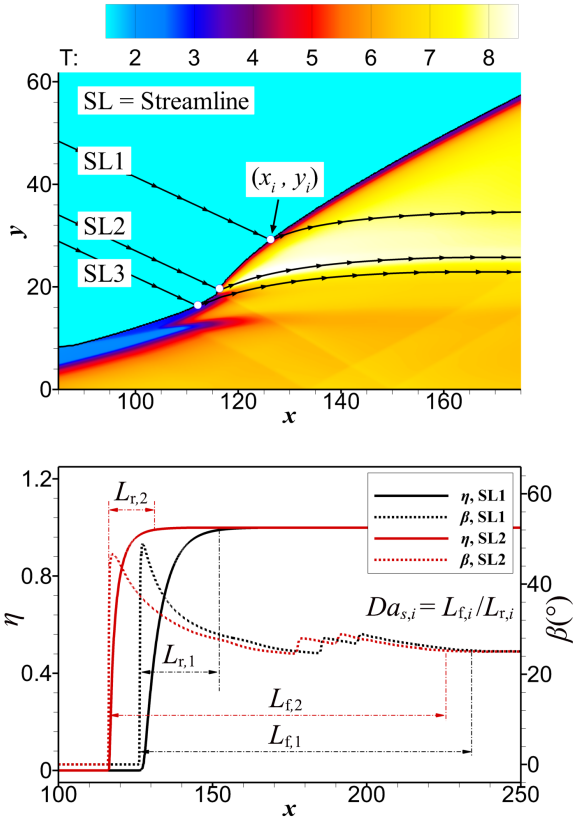

FIG. 11. ODW with $M_0 = 6.5$, $\theta = 25°$ and $k_R = 1.1$, (a) temperature field with three streamlines; (b) definition of the flow/reaction length along the streamline.

As shown in Fig. 11(a), the streamline is straight before the ODW surface, and a rapid variation occurs just behind the surface. Along the post-detonation streamline, the flow direction changes gradually to become parallel to the wedge. For a certain streamline, there are two characteristic parameters, i.e., flow length L_f and chemical reaction length L_r. From the dashed curves shown in Fig. 11(b), we can see that if the incident angle of the inflow is transformed to be zero, the downstream streamline angle is getting close to the theoretical value of 25°, in which the flow is in an equilibrium state. While the chemical reaction has finished and the heat release index η approaches to be 1.0. If the ODW surface is fully developed and keeps smooth, the Da_s of the streamline equals 1.0 in theory. The asynchronous relaxations of the flow and chemical reaction present the non-equilibrium features of the curved ODW section. Hence, L_f is

defined by terminating at where the streamline angle reaches 99% of its final equilibrium value, while L_r is defined by terminating at where η reaches 0.99, also 99% of its final value 1.0. Finally, a dimensionless Damköhler number, Da_s, can be defined by the ratio of the characteristic flow length L_f and chemical reaction length L_r; and the flow/reaction coupling analysis could go ahead further.

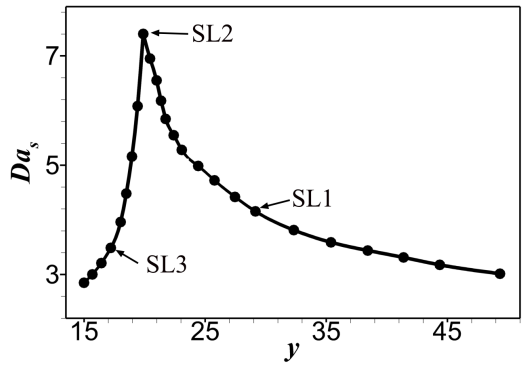

FIG.12 The *Das* as a function of the intersection position y, which corresponds to the simulated ODW with $M_0 = 6.5$, $\theta = 25°$ and $k_R = 1.1$.

Notably, the initiation of a detonation wave is a non-uniform and non-equilibrium process. We have examined plenty of streamlines near the initiation region and every streamline has its own Da_s that is a function of the intersection position (x, y), as shown in Fig. 11. To elaborate on this point, the Da_s vs. y map of the simulated ODW case shown in Fig. 11 is plotted in Fig. 12. The position "y" variation corresponds to different streamlines. The discrete data (y, Da_s) has not only shown the sensitivity of Da_s to the streamlines, but displayed the relaxation of overdriven ODWs. When the intersection position (x, y) of the chosen streamline and ODW front is far away from the initiation region, the flow approaches a uniform and equilibrium state and the ratio Da_s approximately equals to 1.0 in theory. In turn, the ratio Da_s will be greater than 1.0, such as the streamlines shown in Fig. 12, which means the flow across the curved detonation front is in a strongly non-equilibrium state. For the unstable detonation wave, there exist too many irregular structures on the surface. The triple points will form, collide and fade continually, which results in a non-ideal ODW deviating from the equilibrium state. It is difficult to calculate the accurate flow length L_f. The mean value should be considered for the changing detonation surfaces.

APPENDIX B: SHOCK POLAR THEORY BASED ON EQUILIBRIUM STATE ANALYSIS

Considering the constant specific heat approximation[1,9,21,29], for a hypersonic combustible flow past a wedge with an inclination angle θ, the wave angle β of oblique detonation in the finial equilibrium state can be written as:

$$\frac{\tan\beta}{\tan(\beta-\theta)}=\frac{(\gamma+1)M_0^2\sin^2\beta}{\gamma M_0^2\sin^2\beta+1\pm\sqrt{(M_0^2\sin^2\beta-1)^2-2Q(\gamma-1/\gamma)M_0^2\sin^2\beta}} \quad \text{(B1)}$$

where Q is the total chemical energy available in the mixture and has been scaled with RT_0; and γ is the specific heat ratio. Solving the above equation, a typical detonation polar has been displayed in Fig. 13 with a corresponding shock polar for comparison. In the detonation polar, there exist three distinct classes of ODW branches, namely weak under-driven (WU), weak overdriven (WO), strong overdriven (S) ODWs. When the wedge angle θ is less than the detached angle θ_D and greater than the minimum angle θ_{CJ}, we can obtain two solutions (β_W and β_S) in the detonation polar. For a given flow state including the inflow Mach number M_0 and wedge angle θ, there exist a group of wave angles (β_W, β_D and β_S), which are shown in Table I.

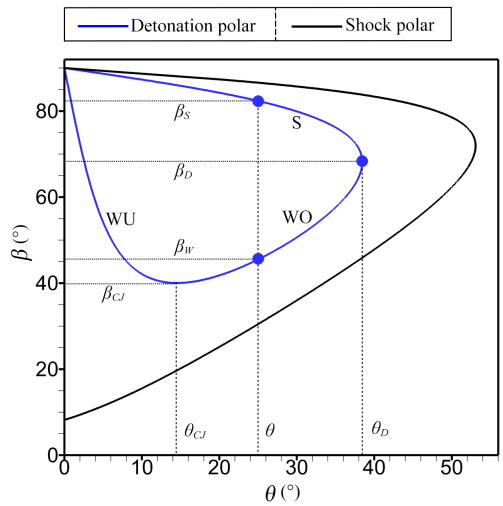

FIG.13. Oblique shock/detonation wave angle depending on wedge angle (M_0=7.0, Q

= 25 or 0, γ =1.2): WU = weak under-driven, WO = weak overdriven, S = strong overdriven.

TABLE I. Different angles from the detonation polar analysis for all simulated cases

M_0	θ (°)	k_R	β_S (°)	β_D (°)	β_W (°)
7.0	25.0	1.0	82.3	68.1	45.5
6.5	25.0	1.0	81.1	67.9	48.9
6.0	25.0	1.0	79.1	67.8	53.5
5.5	25.0	1.0	74.8	68.3	61.3
6.4	25.0	1.0	80.8	67.8	49.7
6.5	24.0	1.0	81.6	67.9	48.0
6.5	25.0	1.1	81.1	67.9	48.9
6.0	25.0	0.4	79.1	67.8	53.5
5.9	25.0	0.4	78.6	67.8	54.7
6.0	23.0	0.4	80.4	67.8	51.7
6.0	25.0	0.5	79.1	67.8	53.5

DATA AVAILABILITY

The data that support the findings of this study are available from the corresponding author upon reasonable request.

REFERENCES

[1] R.A. Gross, "Oblique detonation waves," AIAA J. **1**, 1225–1227 (1963).

[2] G. P. Menees, H. G. Adelman, J. Cambier, and J.V. Bowles, "Wave combustors for trans-atmospheric vehicles," J. Propul. Power **8**, 709–713 (1992).

[3] C. Li, K. Kailasanath, and E. S. Oran, "Detonation structures behind oblique shocks," Phys.

Fluids **6**, 1600–1611 (1994).

[4] C. Viguier, L. F. Figueira da Silva, D. Desbordes, and B. Deshaies, "Onset of oblique detonation waves: comparison between experimental and numerical results for hydrogen-air mixture," Proc. Combust. Inst. **26**, 3023–3031 (1996).

[5] L. F. Figueira da Silva and B. Deshaies, "Stabilization of an oblique detonation wave by a wedge: a parametric numerical study," Combust. Flame **121**, 152–166 (2000).

[6] H. H. Teng and Z. L. Jiang, "On the transition pattern of the oblique detonation structure," J. Fluid Mech. **713**, 659–669 (2012).

[7] J. Y. Choi, D. W. Kim, I. S. Jeung, F. Ma, and V. Yang, "Cell-like structure of unstable oblique detonation wave from high-resolution numerical simulation," Proc. Combust. Inst. **31**, 2473–2480 (2007).

[8] J. Verreault, A. J. Higgins, and R. A. Stowe, "Formation of transverse waves in oblique detonations," Proc. Combust. Inst. **34**, 1913–1920 (2013).

[9] D. Martínez-Ruiz, C. Huete, A. L. Sánchez, and F. A. Williams, "Theory of weakly exothermic oblique detonations," AIAA J. **58**, 236–242 (2020).

[10] M. V. Papalexandris, "A numerical study of wedge-induced detonations," Combust. Flame **120**, 526–538 (2000).

[11] Q. Qin and X. Zhang, "A novel method for trigger location control of the oblique detonation wave by a modified wedge," Combust. Flame **197**, 65–77 (2018).

[12] G. X. Xiang, X. Gao, W. J. Tang, X. Z. Jie, and X. Huang, "Numerical study on transition structures of oblique detonations with expansion wave from finite-length cowl," Phys. Fluids **32**, 056108 (2020).

[13] G. Q. Zhang, S. F. Gao, and G. X. Xiang, "Study on initiation mode of oblique detonation induced by a finite wedge," Phys. Fluids **33**, 016102 (2021).

[14] K. Iwata, S. Nakaya, and M. Tsue, "Wedge-stabilized oblique detonation in an inhomogeneous hydrogen–air mixture," Proc. Combust. Inst. **36**, 2761–2769 (2017).

[15] P. Yang, H. D. Ng, and H. Teng, "Numerical study of wedge-induced oblique detonations in unsteady flow," J. Fluid Mech. **876**, 264–287 (2019).

[16] G. D. Roy, S. M. Frolov, A. A. Borisov, and D.W. Netzer, "Pulse detonation propulsion: challenges, current status, and future perspective," Prog. Energy Combust. Sci. **30**, 545–672 (2004).

[17] Y. Zhu, Z. Pan, P. Zhang, and J. Pan, "Stable detonation characteristics of premixed C_2H_4/O_2 gas in narrow gaps," Exp. Fluids **58**, 112 (2017).

[18] V. Anand and E. Gutmark, "Rotating detonation combustors and their similarities to rocket instabilities," Prog. Energy Combust. Sci. **73**, 182–234 (2019).

[19] Pan, Z., Chen, K., Qi, J., et al.: "The propagation characteristics of curved detonation wave: Experiments in helical channels," Proc. Combust. Int. **37**, 3585–3592 (2019).

[20] Q. Meng, N. Zhao, and H. Zhang, "On the distributions of fuel droplets and in situ vapor in rotating detonation combustion with prevaporized n-heptane sprays," Phys. Fluids **33**, 043307 (2021).

[21] P. Yang, H. Teng, Z. Jiang, and H. D. Ng, "Effects of inflow Mach number on oblique detonation initiation with a two-step induction-reaction kinetic model," Combust. Flame **193**, 246–256 (2018).

[22] W. Xiao, C. Mao, T. Jin, K. Luo, and J. Fan, "Fully resolved simulation of a shockwave

interacting with randomly clustered particles via a ghost-cell immersed boundary method," Phys. Fluids **32**, 066105 (2020).

[23] Y. Zhu, L. Gao, K. H. Luo, J. Pan, Z. Pan, and P. Zhang, "Flame evolution in shock-accelerated flow under different reactive gas mixture gradients," Phys. Rev. E **100**, 013111 (2019).

[24] D. Martínez-Ruiz, C. Huete, A. L. Sánchez, and F. A. Williams, "Interaction of oblique shocks and laminar shear layers," AIAA J. **56**, 1023–1230 (2018).

[25] X. Guo, Z. Zhai, J. Ding, T. Si, and X. Luo, "Effects of transverse shock waves on early evolution of multi-mode chevron interface," Phys. Fluids **32**, 106101 (2020).

[26] K. Ghorbanian and J. D. Sterling, "Influence of formation processes on oblique detonation wave stabilization," J. Propul. Power **12**, 509–517 (1996).

[27] Y. Zhang, Y. Fang, H. D. Ng, and H. Teng, "Numerical investigation on the initiation of oblique detonation waves in stoichiometric acetylene–oxygen mixtures with high argon dilution," Combust. Flame **204**, 391–396 (2019).

[28] H. Teng, C. Tian, Y. Zhang, L. Zhou and H. D. Ng, "Morphology of oblique detonation waves in a stoichiometric hydrogen–air mixture," J. Fluid Mech. **913**, A1 (2021).

[29] D. T. Pratt, J. W. Humphrey, and D. E. Glenn, "Morphology of standing oblique detonation waves," J. Propul. Power **7**, 837–845 (1991).

[30] J. M. Powers and K. A. Gonthier, "Reaction zone structure for strong, weak overdriven, and weak underdriven oblique detonations," Phys. Fluids A **4**, 2082 (1992).

[31] J. Verreault, A. J. Higgins, and R. A. Stowe, "Formation and structure of steady oblique and conical detonation waves," AIAA J. **50**, 1766–1772 (2012).

[32] Y. Zhang, L. Zhou, J. Gong, H. D. Ng, and H. Teng, "Effects of activation energy on the instability

of oblique detonation surfaces with a one-step chemistry model," Phys. Fluids **30**, 106110 (2018).

[33] H. D. Ng, M. I. Radulescu, A. J. Higgins, N. Nikiforakis, and J. H. S. Lee, "Numerical investigation of the instability for one-dimensional Chapman-Jouguet detonations with chain-branching kinetics," Combust. Theory Model. **9**, 385–401 (2005).

[34] Z. L. Jiang, "Dispersion-controlled principles for non-oscillatory shock-capturing schemes," Acta Mech. Sin. **20**, 1–15 (2004).

[35] D. Martínez-Ruiz, L. Scotzniovsky, A. L. Sánchez, and F. A. Williams, "Wedge-induced oblique detonations with small heat release," AIAA Scitech 2021 Forum, AIAA 2021-0287 (2021) .

[36] C. L. Lawson and R. J. Hanson, "Solving least squares problems," Society for Industrial and Applied Mathematics, Philadelphia, US, (1995).

[37] J. Nocedal and S. Wright, "Numerical optimization," Springer Science & Business Media, Berlin, (2006).